*metals*

MDPI

*Article*

# Dislocation Dynamics Model to Simulate Motion of Dislocation Loops in Metallic Materials

**Xinze Tan [1], Enhui Tan [2] and Lizhi Sun [3,*]**

[1] Department of Biomedical Engineering, Columbia University, New York, NY 10027, USA
[2] Bridge Office, Minnesota Department of Transportation, Oakdale, MN 55128, USA
[3] Department of Civil & Environmental Engineering, University of California, Irvine, CA 92697, USA
* Correspondence: lsun@uci.edu; Tel.: +1-949-824-8670

**Abstract:** Dislocation dynamics has been an intensive research subject in materials science and engineering due to the significant roles it plays in plastic deformation and the hardening of metals, fracture mechanics, and the fabrication of semiconductor thin films. However, a long-standing problem from the three-dimensional dislocation dynamics is that the motion and interaction of dislocation loops heavily depend on the loop-segment sizes, which substantially reduces the accuracy of simulation. We herein propose a new three-dimensional dislocation dynamics model together with its physical background. The proposed model incorporates the inherent interactions among differential dislocation segments. The simulation results on motion of Frank–Read sources demonstrate that the proposed model can resolve the paradoxical segment-dependent phenomenon in dislocation dynamics.

**Keywords:** dislocation dynamics; dislocation loop; Frank–Read source; modeling and simulation; metallic materials



**Citation:** Tan, X.; Tan, E.; Sun, L. Dislocation Dynamics Model to Simulate Motion of Dislocation Loops in Metallic Materials. *Metals* **2022**, *12*, 1804. https://doi.org/10.3390/met12111804

Academic Editors: João Manuel R. S. Tavares, José Machado and John D. Clayton

Received: 6 August 2022
Accepted: 20 October 2022
Published: 24 October 2022



## 1. Introduction

Metallic materials contain crystal defects in their microstructures, which can be point, line, surface, or volume defects. These defects locally disturb the regular arrangement of atoms. Their presence, especially the presence of the line defects (dislocation loops), essentially determines the strength and plastic deformation of crystalline solids.

Partly because the macroscopic plastic responses of metals are primarily controlled by the nucleation, motion, annihilation, and interaction of dislocations in them, dislocation dynamics has been of great interest to researchers and engineers in the past several decades. Analytical solutions to this problem are impossible in most cases due to the inherent complexity of dislocation loops. Various discretization techniques are widely employed instead, which are known as discrete dislocation dynamics. With the rapid development of computational technology, a lot of important research work on dislocation dynamics has been made since the 1980s. Dislocation dynamics was first applied to two-dimensional (2D) straight, infinitely long dislocations [1–4], and then to the much more complicated three-dimensional (3D) dislocation loops in the infinite domain [5–20].

While computational methods have been proposed to model the motion, evolution, and interactions of 3D dislocation arrays, an open question associated with these methods is how to discretize dislocation loops, since inappropriate selection of dislocation segments causes unrealistic responses, as indicated by Gómez-García, Devincre, and Kubin [21]. Ghoniem et al. [11] also showed a strange "velocity jump" phenomenon, illustrated in Figure 1a, in which the movements near the two pinning points of a straight dislocation loop can jump as the number of line segments increases. Such an unreasonable phenomenon contradicts with the numerical approaches that finer discretized meshes employ in order to obtain more accurate solutions. As a matter of fact, simulation results are influenced by the artificial selection of the number of segments and meshes, as shown in Figure 1b, which

casts doubts on the reliability of simulations in dislocation dynamics. The current paper aims to investigate the reasons behind such abnormal appearances and to develop a novel model of dislocation motion and dynamics.

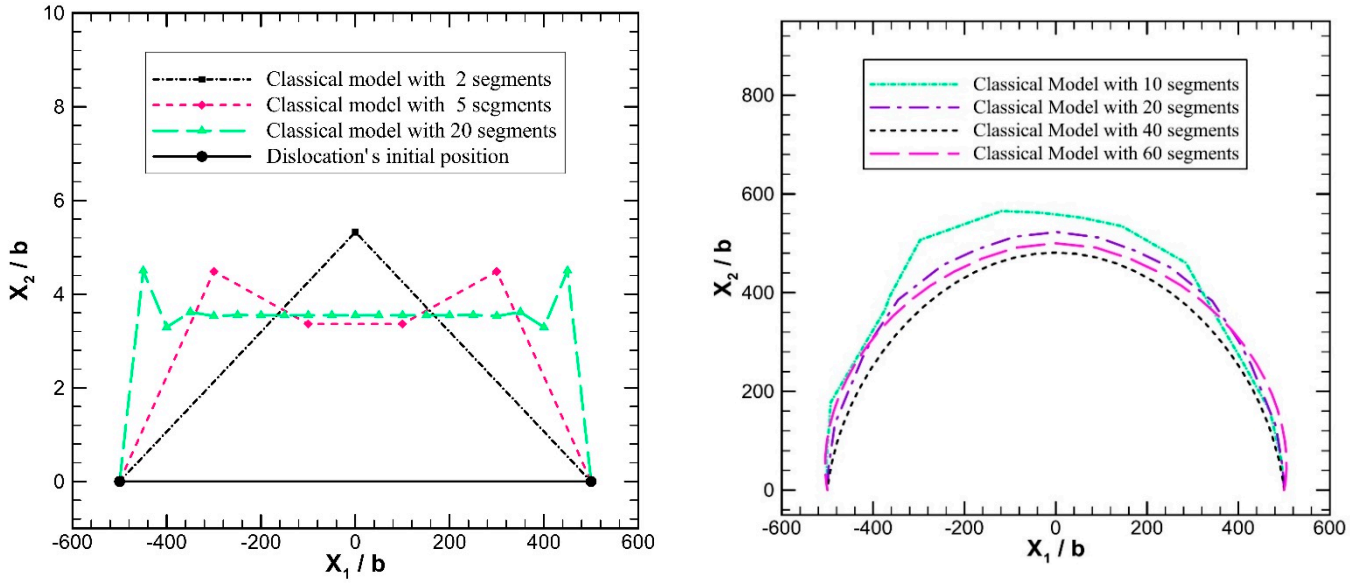


(**a**) (**b**)

**Figure 1.** Simulation results from a classical dislocation dynamics model for a straight dislocation loop: (**a**) the dislocation segment jumps near the pinning points in the first time-step as the number of segment increases; (**b**) dislocation positions are dependent on the number of segments during the dislocation loop's motion and evolution processes.

## 2. Methodology

With a given three-dimensional dislocation loop, the conventional dislocation-dynamics methods are based on the following governing equation [22]:

$$B_{ij}V_j = F_i \tag{1}$$

where $F_i$ ($i$ = 1, 2, 3) represents the local glide force per unit length exerting on the dislocation loop, $B_{ij}$ ($i$, $j$ = 1, 2, 3) is the second-rank tensor of dislocation drag coefficients, and $V_j$ ($j$ = 1, 2, 3) is the local velocity of the dislocation. Furthermore, $B_{ij}V_j$ is also called the drag force of the dislocation. It is noted that all equations are written with tensorial indicial notation (i.e., the free indices take values from 1 to 3 and the repeated indices are summed from 1 to 3 unless explicit statements are indicated [23,24]). From the Peach–Koehler formula [25], glide force $F_i$ can be expressed as follows:

$$F_i = -b_j\sigma_{jk}n_kt_i \tag{2}$$

where $\sigma_{jk}$ is the second-rank stress tensor, $b_j$ the Burgers vector of the dislocation, $n_k$ the unit normal to the slip plane, and $t_i$ the in-plane unit normal to the dislocation loop. It is noted that the Peach–Koehler formula-based glide force $F_i$ is always in the same direction of $t_i$, perpendicular to the dislocation loop. Contributions to the stresses $\sigma_{jk}$ may come from the applied stresses and the self-stresses due to the dislocation loop itself. The self-stresses induced by a dislocation itself is best found using Brown's formula [26] or Gavazza and Barnett's equation [27] to avoid singularity issues.

Mathematically, the combination of Equations (1) and (2) indicates that the dislocation velocity $V_j$ is determined by the glide force $F_i$, as long as the size of the dislocation and applied loads are given. Further investigation shows that the glide force $F_i$ is completely

derived, independent of the velocity variation along the dislocation line. Therefore, Equation (1) is essentially an algebraic equation rather than differential equation, from which the velocity $V_j$ can be calculated without the need of discretization processes. If the entire dislocation loop is segmented into many pieces of lines, the nodes at the ends of segments may jump because of the certain averaging approaches involved. That is the reason why the abnormal appearance occurs in Figure 1a causing the dislocation positions in Figure 1b dependent on the number and size of segments during its motion processes.

From a physical point of view, the abnormal phenomenon that dislocation motion is dependent on segment size is due to the fact that only a minor portion of the interaction between adjacent segments is taken into consideration in Equation (1). In the mechanics theory of dislocations, a dislocation is considered as a continuous tube. Because of the stress field external to the tube, the elastic interaction between adjacent dislocation segments is represented by the contribution of self-stresses in Equation (2). However, as illustrated in Figure 2a, the local interaction due to the core structure of the tube is not taken into account in Equation (2). Such local interactions have been exemplified by the Finnis–Sinclair interatomic potential [28] and the interatomic bondings in dislocation cores [29], implying that the local interactions be taken into account in the framework of dislocation dynamics.

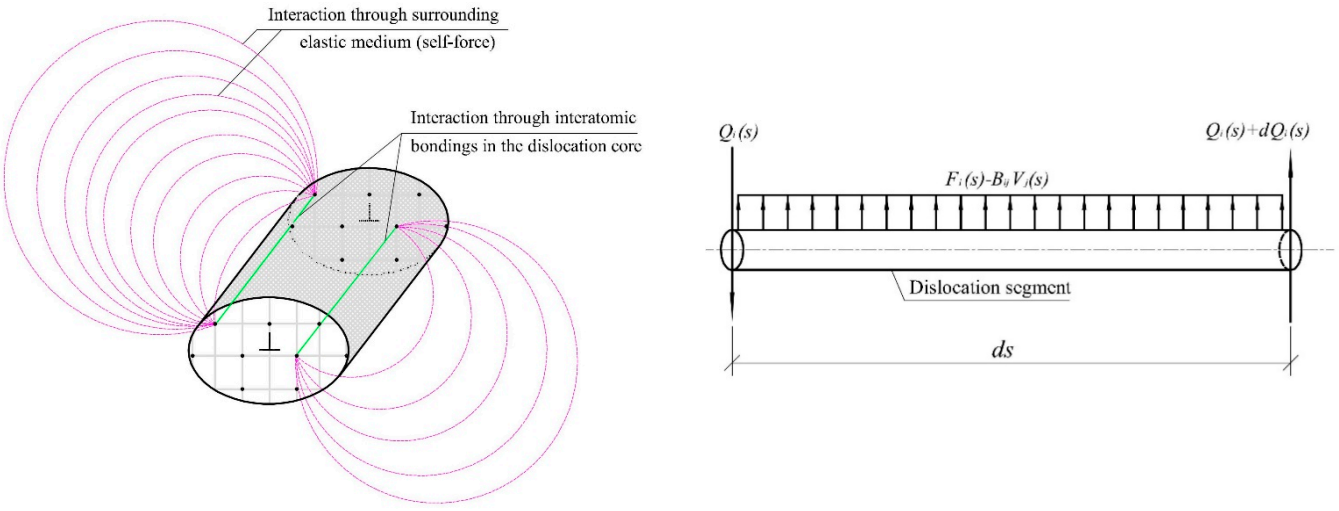


(**a**) (**b**)

**Figure 2.** (**a**) Interactions of adjacent differential dislocation segments can be divided into two parts. (**b**) Free-body diagram of a differential dislocation segment with forces acting on it.

Based on the above arguments, the local interaction can be assumed to adhere to the viscous law as follows:

$$Q_i(s) = \eta_{ij}\frac{\partial V_j(s)}{\partial s} \tag{3}$$

where $Q_i$ signifies the shear force between adjacent differential segments, $\eta_{ij}$ denotes the second-rank tensor of the local interaction of dislocation segments, and $s$ represents a local one-dimensional coordinate along the dislocation loop. From the free-body diagram for a tubed dislocation segment, as shown in Figure 2b, a revised governing equation of dislocation dynamics can be derived as follows:

$$B_{ij}V_j(s) - \eta_{ij}\frac{\partial^2 V_j(s)}{\partial s^2} = F_i(s) \tag{4}$$

It is noted that the above governing equation considers both the elastic and local interactions between dislocation segments.

## 3. Numerical Implementation

Similar to the standard finite element method, the numerical approach applied herein discretizes the dislocation loop into $M$ curved segments, each of which has $M^s$ nodes. The coordinates and velocities at any point on a segment are given as follows:

$$r_i = \sum_{j=1}^{3M^s} N_{ij}(u) r_j^s;\ V_i = \sum_{j=1}^{3M^s} N_{ij}(u) V_j^s \tag{5}$$

where $r_i$ is the coordinate of a point on the segment, ${r_j}^s$ is the node coordinate of the segment, ${V_j}^s$ is the velocity vector of the segment, and $N_{ij}$ $(u)$ is the interpolation function dependent on the parameter $u(-1 \le u \le 1)$. The weak form of Equation (4) for each segment can then be rewritten as follows:

$$\sum_{j=1}^{3M^s} \left( K_{ij}^{s\eta} + K_{ij}^{sB} \right) V_j^s = F_i^s \ (i = 1, 2, \ldots, 3M^s) \tag{6}$$

where $K_{ij}^{s\eta} = \int_{-1}^{1} \eta_{lm} \frac{\partial N_{li}}{\partial s} \frac{\partial N_{mj}}{\partial s} du$, $K_{ij}^{sB} = \int_{-1}^{1} J^2 B_{lm} N_{li} N_{mj} du$, $F_i^s = \sum_{k=1}^{3M^s} \int_{-1}^{1} J^2 N_{ji} N_{jk} F_k^d du$ with $J = \|\partial s / \partial u\|$ being the Jacobian and $F_k^d (i = 1, 2, \ldots, 3M^s)$ as the local force at the nodes. With the assembly processes, the corresponding global equation is obtained as follows:

$$\sum_{j=1}^{3M_P} \left( K_{ij}^{\eta} + K_{ij}^{B} \right) V_j = F_i \ (i = 1, 2, \ldots, 3M_P) \tag{7}$$

where $M_p$ is the total number of nodes of the dislocation loop, and $K_{ij}^{\eta}$ and $K_{ij}^{B}$ are obtained by assembling $K_{ij}^{s\eta}$ and $K_{ij}^{sB}$, respectively. Solving Equation (7) with appropriate constraints on $V_j \left( j = 1, 2, \ldots, 3M_p \right)$, the node velocities, as well as the velocity of the entire dislocation loop, can be computed.

The time span is also discretized into many time steps. If the velocity $V_j$ at time step $t_i$, say, $\left\{ V_j \right\}_{t_i}$, has already been obtained by solving Equation (7), then the dislocation position at the next time step $t_{i+1}$ can be obtained as follows:

$$\left\{ r_j \right\}_{t_{i+1}} = \left\{ r_j \right\}_{t_i} + \left\{ V_j \right\}_{t_i} (t_{i+1} - t_i) \tag{8}$$

## 4. Results and Discussion

The critical stress necessary to activate a Frank–Read source of dislocation and its evolution have been a major topic in the theory of dislocation dynamics. Foreman [30] was the first to employ computer technology to determine the equilibrium shape and critical stress of a Frank–Read source by continuously adjusting node positions until the dislocation reached an equilibrium state. This method, however, cannot simulate the evolution of a Frank–Read source with any great degree of precision. Devincre and Condat [31] applied a 3D dislocation dynamics model to simulate the evolution and evaluate the critical stress of a Frank–Read source. While various dislocation dynamics models have been actively researched since then, the ability to simulate the evolution of dislocations is still limited by the inherent complexity of this problem, as previously indicated in Section 1.

With the newly developed governing equations and numerical scheme derived in this paper, the motion, bowing, evolution, and critical stress of a Frank–Read source are examined herein. Without losing any generality, the parameters are selected as follows: the Burgers vector $b = 2.86$ , the distance between the two pinning points $L = 1000b = 2860$ , shear modulus $\mu = 71.0$ GPa, Poisson's ratio $\nu = 0.3333$, drag coefficient $B = 1.0 \times 10^{-4}$ Pa·S, local interaction $\eta = 1.0 \times 10^{-20}$ N·S, and time step $\Delta t = 5.0 \times 10^{-12}$ s (second). Figure 3 shows the direct comparison between the current model and classical dislocation dynamics simulation. Figure 3a shows the shapes of a Frank–Read source after the first-time step

simulated using the classical model and the current model, respectively, demonstrating that the current model is robust, while the classical simulation maintains a peculiar "velocity jump" phenomenon at the beginning steps. Also, Figure 3b shows that the current model quickly stabilizes and converges when the number of dislocation segments approaches 20; yet, for the classical model, dislocation positions are heavily dependent on the number of segments during the motion and evolution processes of the Frank–Read source.

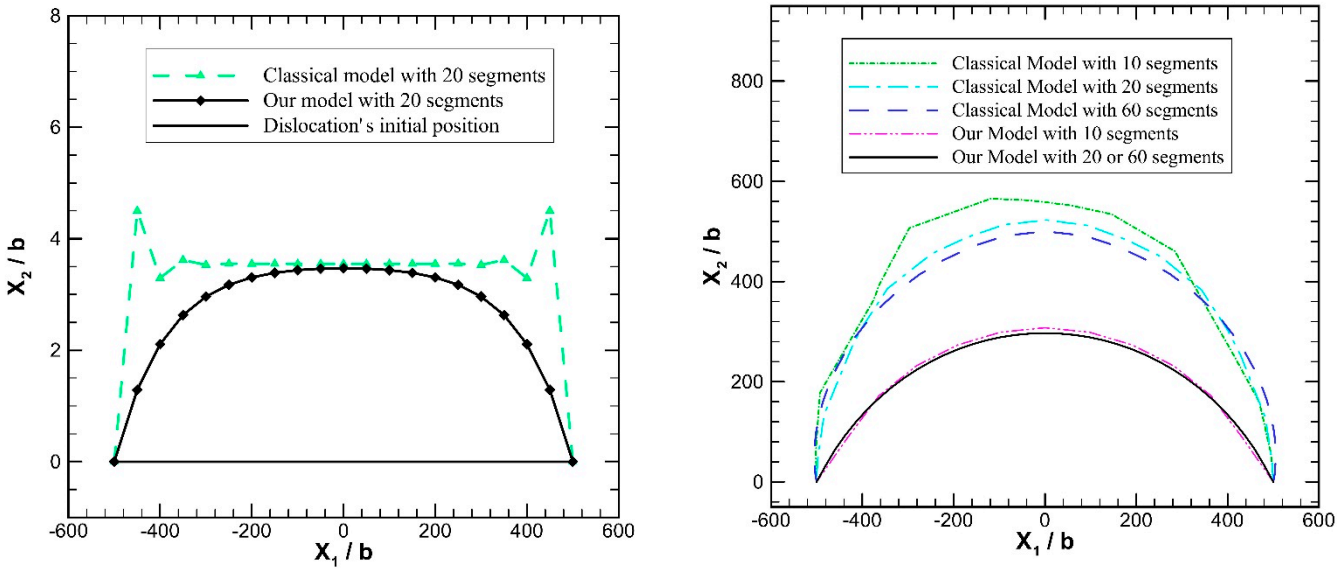


(**a**) (**b**)

**Figure 3.** Comparison between the current model and classical dislocation dynamics simulation at (**a**) the first-time step of a straight dislocation loop and at (**b**) the 200th time-step during the evolution process of the dislocation.

Furthermore, Figure 4 illustrates the simulation results for the equilibrium bowing-out of the Frank–Read source and its motion and evolution processes. Specifically, Figure 4a demonstrates that, for an initial edge dislocation Frank–Read source subject to an applied stress no greater than the critical stress, the equilibrium positions are dependent on applied stresses. The results are in good agreement with those given by Foreman [30]. If the applied stress is greater than the critical stress, the annihilation mechanism of Frank–Read source is activated. The entire dislocation evolution of such a case is shown in Figure 4b, exhibiting that the dislocation decelerates, accelerates, and then remains at an almost constant speed during the entire expansion process. For a Frank–Read source with a smaller length, our model can still converge quickly and accurately predict the critical stress, as shown in Figure 4c. The effect of local interaction in a dislocation core is also investigated with the change of η values of the Frank–Read source, showing in Figure 4d that weak interaction yields early evolution and annihilation of the Frank–Read dislocation loop.

Figure 5 demonstrates the relationship between calculated critical stresses and segment numbers. The new model demonstrates excellent stability for various segment sizes. The calculated critical stresses quickly converge to the solution given by Foreman [30], while the results from the classical model heavily depend on the segment size and the artificial 'manipulations' during the simulation processes.

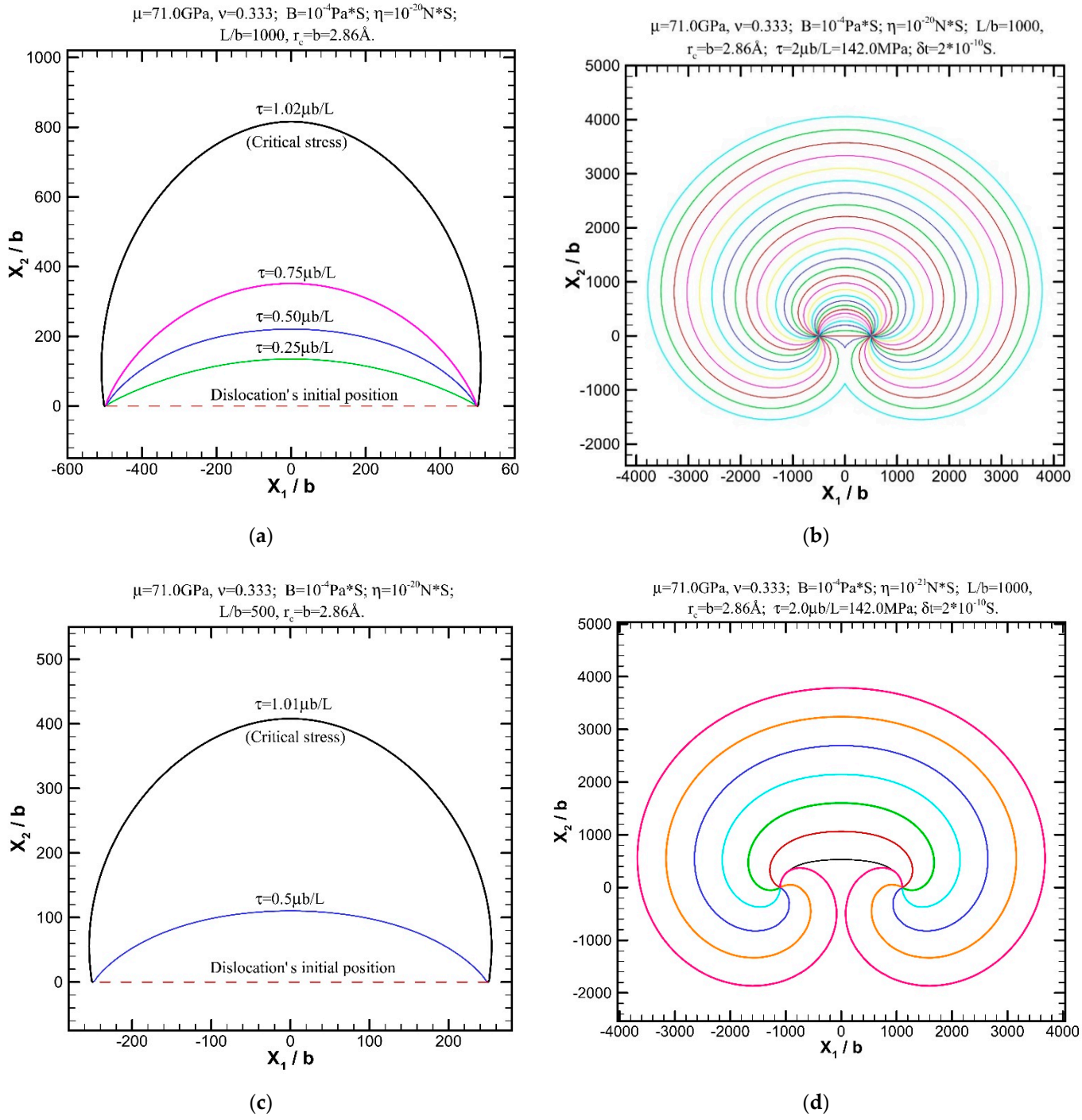


**Figure 4.** Simulation results for equilibrium bowing-out of the Frank–Read source and its motion and evolution processes: (**a**) Equilibrium positions of an initial edge dislocation of relative length $L/b$ = 1000 under different applied stresses; (**b**) Evolution of the dislocation with strong local interaction under the action of an applied stress of 2.0 μb/L; (**c**) Equilibrium positions of the dislocation of relative length $L/b$ = 500 under different applied stresses; (**d**) Evolution of the dislocation with weak local interaction under the action of an applied stress of 2.0 μb/L. The time between neighboring evolution lines is $\delta t = 2.0 \times 10^{-10}$ S.

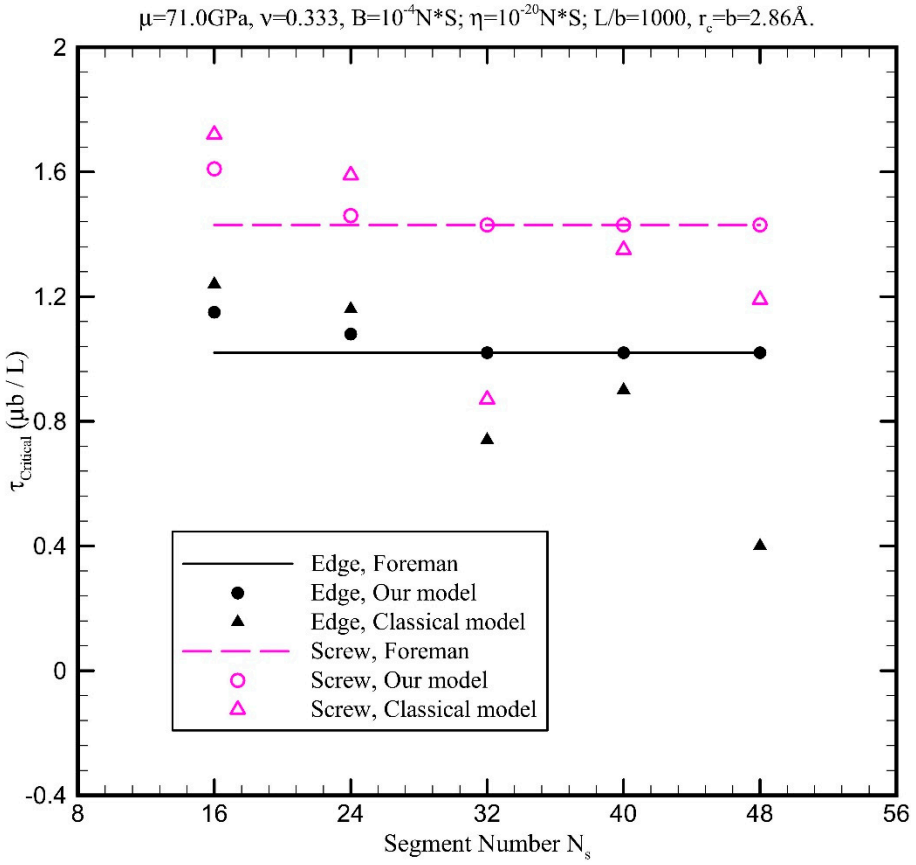


**Figure 5.** Relationship between calculated critical stresses and segment numbers.

## 5. Conclusions

In our proposed model, we fully take into account the local interaction between dislocation segments to resolve the long-standing paradoxical problem mentioned in the literature [11,21]. As expected, the determinations of equilibrium shape and critical stress are insensitive to the values of drag coefficient tensor $B_{ij}$ and local interaction tensor $\eta_{ij}$ of the dislocation, provided that they vary within a reasonable range. For example, it is $10^{-5} \sim 10^{-3}$ Pa·S for $B_{ij}$ and $10^{-24} \sim 10^{-19}$ N·S for $\eta_{ij}$ in our simulation of the Frank–Read source. In contrast, the evolution profiles of the dislocation from the conventional models are heavily dependent on the values of $B_{ij}$. Under the action of applied stresses larger than, but comparable to, the critical stress, the dislocation expansion speed varies greatly in the multiplication process. However, the dislocation velocity does not vary appreciably if the applied stress is sufficiently large. It is interesting that if we divide $\eta = 10^{-20}$ N·S by the cross-sectional area of the dislocation tube, we can find $\eta / \pi r_c^2 = 3.89 \times 10^{-2}$ Pa·S, which falls into the normal range of material viscosity coefficients. It can be surmised that the intrinsic local interaction within a dislocation loop may be determined with the molecular dynamics methods. Yet, experimental approaches to determining the interaction parameter $\eta_{ij}$ would surely be of significant benefit. Finally, it should be noted that the new dislocation dynamics model applies not only to the Frank–Read sources but also to general dislocation dynamics problems.

**Author Contributions:** X.T.: Investigation, Formal Analysis, Data Curation, Writing—Reviewing and Editing. E.T.: Methodology, Investigation, Data Curation, Writing—Original Draft Preparation. L.S.: Conceptualization, Methodology, Supervision, Writing—Reviewing and Editing. All authors have read and agreed to the published version of the manuscript.

**Funding:** This study was partly supported by the U.S. National Science Foundation under Grant No. DMR 0113172.

**Institutional Review Board Statement:** Not applicable.

**Informed Consent Statement:** Not applicable.

**Data Availability Statement:** The data that support the findings of this study are available from the corresponding author upon reasonable request.

**Conflicts of Interest:** The authors declare no conflict of interest.

## References


1. Lepinoux, J.; Kubin, L.P. The dynamic organization of dislocation structures: A simulation. *Scr. Metall.* **1987**, *21*, 833–838. [CrossRef]
2. Amodeo, R.J.; Ghoniem, N.M. Dislocation dynamics I, a proposed methodology for deformation micromechanics. *Phys. Rev. B* **1990**, *41*, 6958–6967. [CrossRef] [PubMed]
3. Amodeo, R.J.; Ghoniem, N.M. Dislocation dynamics I, applications to the formation of persistent slip bands, planar arrays, and dislocation cells. *Phys. Rev. B* **1990**, *41*, 6968–6976. [CrossRef] [PubMed]
4. Van der Giessen, E.; Needleman, A. Discrete dislocation plasticity: A simple planar model. *Model. Simul. Mater. Sci. Eng.* **1995**, *3*, 689–735. [CrossRef]
5. Kubin, L.P.; Canova, G.; Condat, M.; Devincre, B.; Pontikis, V.; Brechet, Y. Dislocation microstructures and plastic flow: A 3D simulation. *Solid State Phenom.* **1992**, *23–24*, 455–472. [CrossRef]
6. Schwarz, K.W.; Tersoff, J. Interaction of threading and misfit dislocations in a strained epitaxial layer. *Appl. Phys. Lett.* **1996**, *69*, 1220–1222. [CrossRef]
7. Schwarz, K.W. Interaction of dislocations on crossed glide planes in a strained epitaxial layer. *Phys. Rev. Lett.* **1997**, *78*, 4785–4788. [CrossRef]
8. Tang, M.; Kubin, L.P.; Canova, G.R. Dislocation mobility and the mechanical response of b.c.c. single crystals: A mesoscopic approach. *Acta Mater.* **1998**, *46*, 3221–3235. [CrossRef]
9. Zbib, H.M.; Rhee, M.; Hirth, J.P. On the plastic deformation and the dynamics of 3D dislocations. *Inter. J. Mech. Sci.* **1998**, *40*, 113–127. [CrossRef]
10. Ghoniem, N.M.; Sun, L.Z. Fast-sum method for the elastic field of three-dimensional dislocation ensembles. *Phys. Rev. B* **1999**, *60*, 128–140. [CrossRef]
11. Ghoniem, N.M.; Tong, S.-H.; Sun, L.Z. Parametric dislocation dynamics: A thermaldynamics-based approach to investigations of mesoscopic plastic deformation. *Phys. Rev. B* **2000**, *61*, 913–927. [CrossRef]
12. Diaz de la Rubia, T.; Zbib, H.M.; Khraishi, T.A.; Wirth, B.D.; Victoria, V.; Caturla, M.J. Multiscale modeling of plastic flow localization in irradiated materials. *Nature* **2000**, *406*, 871–874. [CrossRef] [PubMed]
13. Cai, W.; Bulatov, V.V. Mobility laws in dislocation dynamics simulations. *Mater. Sci. Eng. A* **2004**, *387–389*, 277–281. [CrossRef]
14. Cui, Y.; Ghoniem, N.M. Influence of Size on the Fractal Dimension of Dislocation Microstructure. *Metals* **2019**, *9*, 478. [CrossRef]
15. Gao, S.; Yang, Z.; Grabowski, M.; Rogal, J.; Drautz, R.; Hartmaier, A. Influence of Excess Volumes Induced by Re and W on Dislocation Motion and Creep in Ni-Base Single Crystal Superalloys: A 3D Discrete Dislocation Dynamics Study. *Metals* **2019**, *9*, 637. [CrossRef]
16. Fan, H.; Wang, Q.; El-Awady, J.A.; Raabe, D.; Zaiser, M. Strain rate dependency of dislocation plasticity. *Nat. Commun.* **2021**, *12*, 1845. [CrossRef]
17. Muraishi, S. Internal Stress and Dislocation Interaction of Plate-Shaped Misfitting Precipitates in Aluminum Alloys. *Materials* **2021**, *14*, 5811. [CrossRef]
18. Zheng, H.; Liu, J.; Muraishi, S. Dislocation Topological Evolution and Energy Analysis in Misfit Hardening of Spherical Precipitate by the Parametric Dislocation Dynamics Simulation. *Materials* **2021**, *14*, 6368. [CrossRef]
19. Pachaury, Y.; Po, G.; El-Azab, A. Discrete Dislocation Dynamics for Crystal RVEs Part I: Periodic Network Kinematics. *J. Mech. Phys. Solids* **2022**, *163*, 104861. [CrossRef]
20. Schneider, Y.; Rapp, D.-M.; Yang, Y.; Wasserbach, W.; Schmauder, S. Many-scale Investigations of Deformation Behavior of Polycrystalline Composites: II Micro-Macro Simultaneous FE and Discrete Dislocation Dynamics Simulation. *Materials* **2022**, *15*, 2852. [CrossRef]
21. Gómez-García, D.; Devincre, B.; Kubin, L.P. Dislocation dynamics in confined geometry. *J. Comput.-Aided Mater. Des.* **1999**, *6*, 157–164. [CrossRef]
22. Bulatov, V.V.; Cai, W. *Computer Simulations of Dislocations*; Oxford University Press: Oxford, UK, 2006.
23. Yin, H.M.; Sun, L.Z. Magnetoelasticity of chain-structured ferromagnetic composites. *Appl. Phys. Lett.* **2005**, *86*, 261901. [CrossRef]
24. Liu, H.T.; Sun, L.Z.; Ju, J.W. Elastoplastic modeling of progressive interfacial debonding for particle-reinforced metal-matrix composites. *Acta Mech.* **2006**, *181*, 1–17. [CrossRef]
25. Peach, M.; Koehler, J.S. The forces exerted on dislocations and the stress fields produced by them. *Phys. Rev.* **1950**, *80*, 436–439. [CrossRef]
26. Brown, L.M. The self-stress of dislocations and the shape of extended nodes. *Phil. Mag.* **1964**, *10*, 441–466. [CrossRef]

27. Gavazza, S.D.; Barnett, D.M. The self-force on a planar dislocation loop in an anisotropic linear-elastic medium. *J. Mech. Phys. Solids* **1976**, *24*, 171–185. [CrossRef]
28. Finnis, M.W.; Sinclair, J.E. A simple empirical N-body potential for transition metals. *Phil. Mag. A* **1984**, *50*, 45–55. [CrossRef]
29. Telling, R.H.; Ewels, C.P.; El-Barbary, A.A.; Heggie, M.I. Wigner defects bridge the graphite gap. *Nat. Mater.* **2003**, *2*, 333–337. [CrossRef]
30. Foreman, A.J.E. The bowing of a dislocation segment. *Phil. Mag.* **1967**, *15*, 1011–1021. [CrossRef]
31. Devincre, B.; Condat, M. Model validation of a 3D simulation of dislocation dynamics: Discretization and line tension effects. *Acta Metall. Mater.* **1992**, *40*, 2629–2637. [CrossRef]